International Journal of Coal Geology 132 (2014) 23–37

Contents lists available at ScienceDirect

International Journal of Coal Geology

journal homepage: www.elsevier.com/locate/ijcoalgeo

Topographic influence on stability for gas wells penetrating longwall mining areas

Shun Liang [a,b], Derek Elsworth [b], Xuehua Li [a,*], Dong Yang [c]

[a] State Key Laboratory of Coal Resource and Mine Safety, School of Mines, China University of Mining and Technology, Xuzhou, Jiangsu 221008, China
[b] EMS Energy Institute, G3 Center and Energy and Mineral Engineering, Pennsylvania State University, University Park, PA 16802, USA
[c] Institute of Mining Technology, Taiyuan University of Technology, Taiyuan, Shanxi 030024, China

ARTICLE INFO

Article history:
Received 21 April 2014
Received in revised form 11 July 2014
Accepted 11 July 2014
Available online 17 July 2014

Keywords:
Well stability
Topography
Longwall mining
Distortion
Shear offset
Delamination

ABSTRACT

Gas wells penetrating longwall mining areas are prone to fail by shear and distortion due to vulnerability to ground movements caused by coal mining, especially when they pierce layered strata. This work explores the influence of topography on stability for shale gas wells piercing a longwall pillar after sequential removal of the flanking panels. We examine the magnitudes of shear offsets, longitudinal distortions, delamination, lateral and vertical strains along the vertical well trajectories through a longwall pillar and as a result of mining, and evaluate their impact upon the anticipated performance and stability of the wells. Results indicate that the presence of weak interfaces separating monolithic beds is a crucial factor that modulates wellbore instability. Contrast between benign relief and incised surface topography amplifies shear offsets for wells in the overburden by ~20–30%. Well distortions are largest close to the surface or hilltop for mining at shallow depths (100 m) and migrate downwards with an increase in panel depths reaching a maximum in the vicinity of the seam. Tensile failure is more likely to occur for gas wells penetrating the overburden with incised topography, especially for the case with a higher ratio of hill height to the thickness of overburden below the valley floor, with a largest delamination of 42 mm. Incised topography does not cause a significant change in magnitude for axial distortions along well trajectories (limited to $\pm 3 \times 10^{-3}$) but does elevate lateral strains over the horizontal case to different extents. For all topographic conditions, lateral shear offsets and various strains are largest for boreholes that cross the pillar closest to the panel rib and reduce monotonically towards the gateroad, where both the shear offsets and axial distortions reduce to about one-fifth (horizontal) and one-tenth (incised) of the maximum at 7.5 m inboard of the gateroad. Well deformations are most severe when mining is shallow <100 m, then moderate when mining at an intermediate depth ~200 m, and then become large again as the seam deepens >300 m. The spread in the distribution of strain magnitudes between the five horizontal trajectories through the pillar all converge when mining is deeper.

1. Introduction

Gas wells are conduits for the transmission of shale gas, coalbed methane and other natural gas resources from the reservoir to the surface. In regions where the gas resource underlies mineable coal seams, the recovery of that coal may jeopardize the integrity of the well even if an unmined buffer-region is left around the well. This is especially the case where high extraction mining, such as longwall mining, is used as a method of recovery. In this instance the integrity of the wells may be affected by deformation in the overburden, underburden and coal that both precede and follow proximal mining. This issue has been recognized for example in the Pennsylvania Mining Act of 1957 where a barrier pillar surrounding a pre-existing well is required to be of 200,000 ft^2 in tributary area. However, where the recovery is by full extraction (longwall) mining, it is not always feasible to leave an equiaxed (square) pillar due to both mining logistics and the layout of adjacent panels. In this work we examine the rationale for the dimensioning of protective barrier pillars to enable both effective mining and the safe extraction of gas. In addition, the prevention of well failures is important in coal-seam degassing (Karacan et al., 2011; Whittles et al., 2007) where, absent drainage, the accumulation of methane may be significant (Burrel and Friel, 1996; Kral et al., 1998) and these and also gob gas ventholes (GGVs) are important (Karacan, 2013). The effects on gas drainage wells installed prior to mining are clearly greater than for those installed into the gob post-mining — although the general issues of well stability is similar. In this work we examine the rationale for gas well stability under the effects of longwall mining and explore the influence of both topography and seam depth to enable both effective mining and the safe extraction of gas.

A variety of studies have examined the stability of boreholes although most of these have examined the influence of the drilling process and its influence on the resulting stability of the well. These have concentrated on evaluating drilling design, including the provision

* Corresponding author. Tel.: +86-13952196864; fax: +86-516-83590505.
E-mail address: lsxh2001@126.com (X. Li).

http://dx.doi.org/10.1016/j.coal.2014.07.008
0166-5162/

of mud weight and typically assuming that the rock material is linear elastic, homogeneous, and isotropic in deformability and in strength (Bradley, 1979; Santarelli et al., 1986) and extending these analyses to anisotropic strength representing shales and phyllites (Aadnoy, 1988; Ajalloeian and Lashkaripour, 2000; Aoki et al., 1993; Chenevert and Gatlin, 1965; Donath, 1964; Lee et al., 2012; McLamore and Gray, 1967; Niandou et al., 1997; Ong and Roegiers, 1993; Ramamurthy et al., 1993; Tien et al., 2006). Borehole failure mechanisms are also important in determining the integrity of the well (Aadnoy and Chenevert, 1987; Gough and Bell, 1981; Haimson and Song, 1993; Tan and Willoughby, 1993; Tan et al., 1998; Zheng et al., 1989; Zoback et al., 1985) and may also be used to determine the orientation of in situ stresses. Failure is also influenced by rock lithology and the physical-mechanical or chemical–mechanical interactions between clay minerals and drilling fluids or groundwater (Hale et al., 1993; Tan et al., 1996; Van Oort et al., 1994; Zeynali, 2012), but these effects may be minimized by the application of improved drilling methods (Bennion et al., 1996; Bjornsson et al., 2004; Clancey et al., 2007; Supon and Adewumi, 1991) to maximize the effectiveness of drilling.

Despite a significant number of studies relating to well stability for hydrocarbon wells, relatively fewer results are available to define stability under the influence of strata movement and control, or of the effects of pillar crushing. One reason is that the importance of unconventional natural gas reservoirs underlying mineable coal seams has only become an important issue relatively recently (Wang et al., 2013). However, the evaluation of stability for wells piercing minable coal seams may draw on a significant body of work related to the evaluation of the performance of gob gas ventholes (Karacan, 2009a, 2009b; Karacan and Goodman, 2009; Karacan and Olea, 2013), the failure modes of the surface venthole casing during longwall mining (Chen et al., 2012), localization of mining-induced horizontal fractures along rock layer interfaces in overburden (Palchik, 2005), the influence of coal mining on ground-water supplies (Elsworth and Liu, 1995; Liu and Elsworth, 1997, 1999) and the influence of topography on horizontal deformations (Gebauer et al., 2009) adjacent to the mined panels. Despite these contributions, few analyses exist on the topographic influence on well stability for gas wells penetrating longwall mined seams.

This study examines the stability of wells piercing a horizontal seam and subject to sequential mining first on one side and then the other (Fig. 1). In particular, we incorporate the influence of topography above the mined panels and examine the lateral and vertical strains, horizontal shear and vertical delamination displacements and vertical distortions applied along the candidate paths of wells that extend from the surface/hilltop, through the pillar and to depth. We presume the rock to be laminated and capable of separation at bedding interfaces as a representation of mixed sandstone shale sequences in the overburden and underburden. We use this analysis to evaluate areas where the wellbore is prone to collapse or more specifically disruption by shear offset.

2. Mechanistic model

We idealize the subsurface as a deformable medium comprising laminated units with a slip interface, as shown in Fig. 2. The model closely replicates the morphology of interbedded shales and sandstones adjacent to the coal seams with the deformability properties of the units and interfaces controlling the response. We examine the distribution of displacements and strains along a vertical well trajectory, as induced by longwall mining, and evaluate their impact upon the anticipated performance and stability of the wells.

2.1. Strata deformation and distortion

We follow the distortion, tension and compression, delamination, and lateral shear offsets that occur at interfaces between alternating layers of hard and soft strata. This shear slippage and distortion represents the anticipated failure mode for gas wells that traverse the pillar between longwall panels. Compared with compaction in the vertical direction, shear displacement and axial distortion are likely more damaging to wellbores — although all modes may be examined. We represent this interface between layers of alternating mechanical properties by an interface element (Fig. 2) where the elastic distortion, ε_e, irrecoverable shear slip distortion, ε_i, and total distortion, $\varepsilon_t = \varepsilon_e + \varepsilon_i$ are defined as (Fig. 2):

$$\begin{aligned} \varepsilon_e &= \frac{U_x}{d} = \frac{U_{ij} - U_{i(j-1)}}{d} \\ \varepsilon_i &= \frac{\Delta U}{\Delta d} = \frac{U_{i(j+1)} - U_{ij}}{\Delta d} \\ \varepsilon_t &= \frac{T_x}{d} = \frac{U_{i(j+1)} - U_{i(j-1)}}{d} \end{aligned} \tag{1}$$

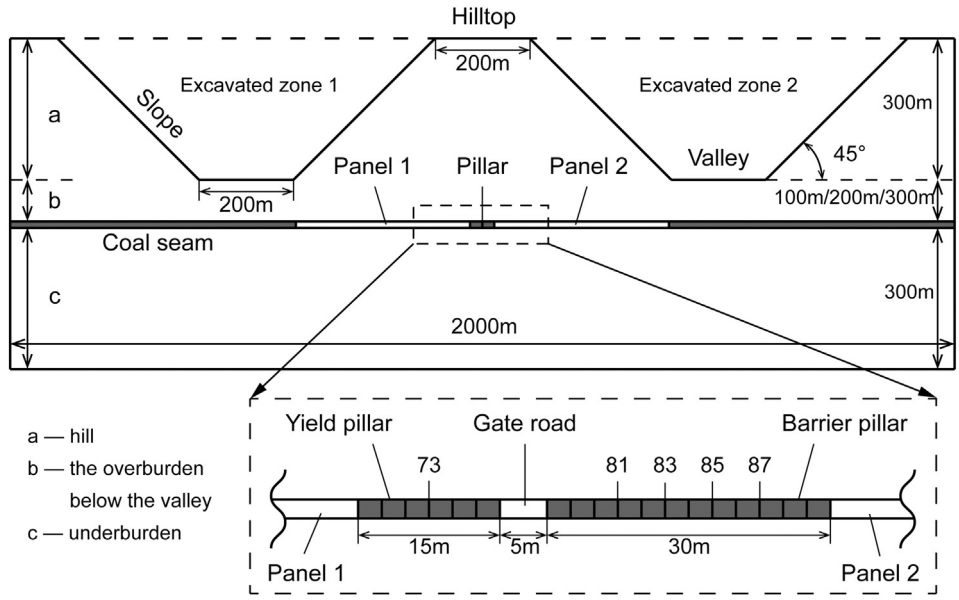

Fig. 1. Two dimensional model with a 2 m thick coal seam at an elevation of 100/200/300 m below the valley-base and with twin panels flanking a central pillar (Pillar geometry between the twin extracted panels is shown in the excerpted frame. Panel 1 is removed first and then panel 2 is also removed afterwards. Pillar widths are in meters and correspond to multiples of element widths of 2.5 m. Numbers refer to grid points in the yield pillar (70–76), intervening gate road (76–78) and the barrier pillar (78–90)).

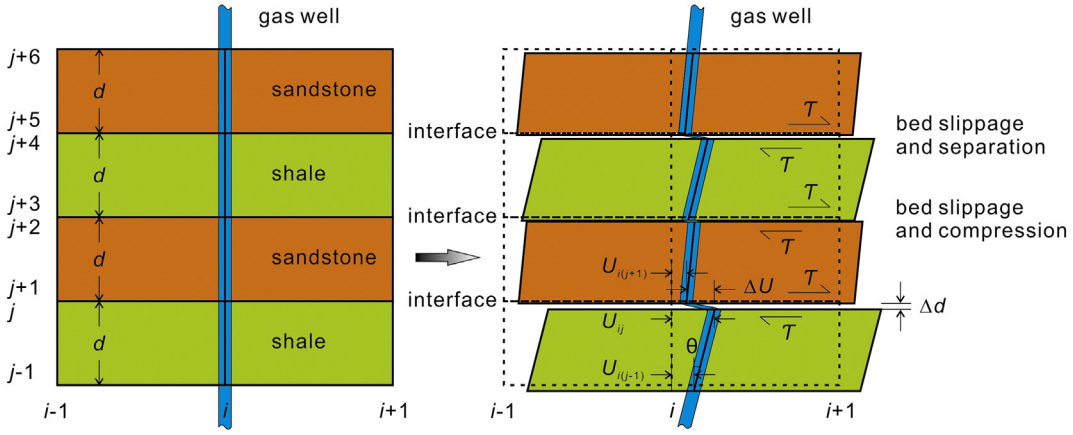

Fig. 2. Typical deformation of a well in and between layers of alternating soft shale and stiff sandstone as the well is distorted by the strata after coal mining (with slip interfaces between alternating layers).

in terms of elastic shear offset, U_x, relative slip offset, ΔU, total offset, $T_x = U_x + \Delta U$ and normalized over the bed thicknesses, d or Δd, referring to the separating distance between layers. U_{ij} refers to the lateral shear (horizontal) displacement of node (i, j), with a similar meaning for $U_{i(j-1)}$ and $U_{i(j+1)}$ in Fig. 2.

2.2. Failure criterion at interfaces

The deformation response is conditioned primarily by the yield behavior as characterized by the Mohr–Coulomb properties of cohesion and friction and the stiffness of the interface. The Mohr–Coulomb criterion is defined as:

$$\tau = c + \sigma_n \tan\phi \tag{2}$$

where, τ is the shear strength, c is the cohesion, σ_n is the normal stress and ϕ is the angle of internal friction. This can also be expressed in the form:

$$\sigma_1 = \frac{1+\sin\phi}{1-\sin\phi}\sigma_3 + \frac{2c\cos\phi}{1-\sin\phi} \tag{3}$$

where, σ_1 and σ_3 are the peak vertical stress and confining stress, respectively. This criterion assumes that a shear failure plane is developed in the rock material at the most critical orientation. When the stresses developed on the failure plane satisfy the shear strength condition, rock failure occurs.

2.3. Interface stiffness

One key behavior that will influence the distortion applied to the vertical wellbore is the presence of shear offsets at the bed interfaces and delamination. An interface is represented with normal and shear stiffness between two planes which may contact or separate as shown in Fig. 3 (FLAC2D, User's Manual, 2002), in which, S is the slider shear strength and T the tensile strength, K_n and K_s are the normal and shear stiffnesses, and L_n and L_m separately refer to the length associated with grid point N and M. More detailed information about this model is available in the FLAC2D manual.

Through maintaining a list of the grid points that lie on each side of any particular surface, each point is taken, in turn, and checked for contact with its closest neighboring point on the opposite side of the interface (FLAC2D, User's Manual, 2002). Referring to Fig. 3, for example, grid point N is checked for contact on the segment between M and P. If contact is detected, the normal, n, to the contact, N, is computed, and a "length", L, defined for the contact along the interface belonging to N, where L is equal to half the distance to the nearest grid point to the left plus half the distance to the closest grid point to the right, irrespective of whether the neighboring grid point is on the same side of the interface or on the opposite side. In this way, the entire joint is divided

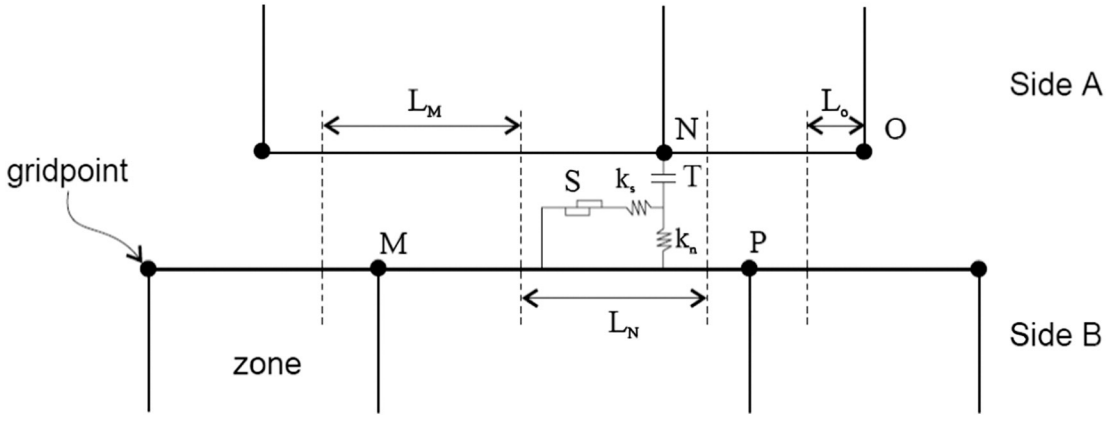

Fig. 3. An interface represented by two blocks (sides A and B), connected by shear (K_s) and normal (K_n) stiffnesses (The dashed line placed halfway between adjacent grid points denotes limits for joint segments) (FLAC2D, User's Manual, 2002).

into contiguous segments, each controlled by a grid point. The incremental relative displacement vector at the contact point is resolved into the normal and shear directions and the total normal (F_n) and shear (F_s) forces can be determined by the following equations:

$$\begin{aligned} F_n^{(t+\Delta t)} &= F_n^{(t)} - K_n \Delta U_n^{(t+\Delta t/2)} L \\ F_s^{(t+\Delta t)} &= F_s^{(t)} - K_s \Delta U_s^{(t+\Delta t/2)} L \end{aligned} \tag{4}$$

or be expressed in matrix form as (Ardeshiri and Yazdani, 2008):

$$\begin{Bmatrix} \Delta F_n \\ \Delta F_s \end{Bmatrix} = \begin{bmatrix} K_n & 0 \\ 0 & K_s \end{bmatrix} \cdot \begin{Bmatrix} \Delta U_n L \\ \Delta U_s L \end{Bmatrix} \tag{5}$$

where, ΔU_n and ΔU_S are separately the displacement increment of the interface element in the normal direction and of a segment of interface element in the tangential direction and L is the segment length of the interface element.

There are two conditions of the weak plane between alternating layers, which can be determined by the following criteria:

(1) Coulomb shear-strength — the Coulomb shear-strength criterion limits the shear force by the following relation:

$$F_{s\max} = cL + \tan\phi F_n. \tag{6}$$

If the criterion is satisfied (i.e., if $|F_s| \geq F_{smax}$), then $F_s = F_{smax}$, with the sign of shear preserved.

(2) Tensile yield condition:

$$F_t = \sigma_t - t \tag{7}$$

where, σ_t is the tensile stress acting on the interface and t is the tensile strength of the interface. If $F_t \geq 0$, then the interface breaks and the shear and normal forces are set to zero. In this application the tensile strength of the interface is zero.

3. The topographic geological model

3.1. Basic assumptions

A variety of factors affect the stability of gas wells that pass through the coal seams that will be mined as proximal longwall panels. These factors can be classified into three categories. The first are the geological factors, including overburden characteristics, the magnitude and orientation of in-situ stresses, dip angle of beds, faults and other geological formations, topography and groundwater conditions. The second are factors relating to mining geometry and including seam thickness, depth, mining method, advance rate and orientation of panels, time interval post-mining, panel size and pillar size. The third are features of the well construction including drilling method, drilling fluids, borehole orientation and casing material and performance. Here we focus on the influences of topography for a given longwall mining method on the distortions in the overburden and presumed level of distress applied to the cased well. We consider all strata as elastic–plastic materials where the plastic response is provided at the interface between layered strata. Furthermore, we neglect any added resistance to distortion by the well casing, as this is a trivial influence relative to the motive distortions of the strata.

3.2. Geological model and parameters

We use the finite difference analysis program FLAC, which is capable of modeling large displacements for continuous media, to build the topographic geological model. Interface elements are employed in this model to represent weak planes between laminated strong and weak layers on which sliding and separation may occur. In this work, emphasis is placed on the effects of such horizontal weak planes, while the influence of vertical through-going fractures is not considered. This is a simplification but the presence of weak bedding planes are the key features to represent, as illustrated by the validation studies completed against field data. The mining geometry is as shown in Fig. 1 and comprises overburden, coal seam and underburden materials. The model is 2000 m × 402 m ~ 902 m representing a flat-topped hill flanked by two valleys. Valley base and hilltop spans are each 200 m wide and the valley depth is 300 m with a relatively steep slope of 45°. The coal seam is 2 m in thickness, and the overburden from coal seam to the valley-base is 100, 200 and 300 m in thickness in different scenarios. Gas wells are drilled from the hilltop or ground surface to the shale gas reservoir and penetrate the coal seam beneath the hill. The extracted panels are 370 m in width and flank a single central pillar which is divided into a yield pillar (15 m wide) and a barrier pillar (30 m wide) and contains three entries (each entry is 5 m wide). The panels are advanced into the page — in this 2D analysis, each panel is excavated instantaneously and to infinite length — first on the left, then subsequently on the right.

In the analyses the resistance of the casing in arresting the shear displacement between beds is not considered. A simple scaling analysis reveals that the failure-in-bending-resistance of the casing is small in comparison to the couple that must be applied to prevent shear in the beds. Thus this effect is ignored and with no loss of fidelity. In the analysis, the model is first built with the initial surface (Fig. 1), then excavations are conducted in sequence as follows: zones 1 and 2 are elastically excavated (the topographic surface forms) → change the model material from elastic to plastoelastic → the intervening gateroad is excavated (deformations are reset) → excavate panel 1 to equilibrium → excavate panel 2 to final equilibrium.

The lateral and basal boundaries of the model are rollered (zero normal displacement or velocity) and the upper boundary is stress-free. The model has been calibrated against observed and recorded surface subsidence in the Appalachian coalfields — specifically during the undermining of I-79 (Gutierrez et al., 2010) — and calibrated against projected empirical fits to data where subsidence data are not directly available. As apparent in Table 1, these parameter magnitudes are essentially the same for analyses of different depths. Interfaces are set to yield bed thicknesses of 10 m and 20 m for overburden either below or above the valley base, respectively, except for the uppermost layer at the hilltop, which is 30 m in thickness.

The initial condition for the model is met by applying gravity with a lateral stress ratio of unity. The model is run to an initial equilibrium and the gateroad then excavated. Model displacements are then set to zero

Table 1
Parameters of rock mass and interface used in the model.

Lithology	Thickness (m)	Bulk GPa)	Shear (GPa)	Density (Kg/m^3)	Cohesion (MPa)	Friction angle (deg)	Tension (MPa)
Sandstone	30	13.3	8.0	2650	88	30	1.0
Shale	20	3.3	2.0	2300	21	30	0.4
Sandstone	20	13.3	8.0	2650	88	30	1.0
…	Alternating layers of 10 m/20 m thick soft shale and stiff sandstone in overburden under/above the valley-base						
Sandstone	10	13.3	8.0	2650	88	30	1.0
Shale	10	3.3	2.0	2300	21	30	0.4
Coal	2.0	2.3	1.4	1500	1.5	30	0.01
Shale	10	3.3	2.0	2300	21	30	0.4
Sandstone	10	13.3	8.0	2650	88	30	1.0
…	Alternating layers of 10 m thick soft shale and stiff sandstone in underburden						
Property parameters of interface (unglued)							
Ks (GPa)		Kn (GPa)				Friction angle (deg)	
1.7		1.7				20	

Table 2
Location of gas wells as they penetrate the pillar. Wells are taken along the edges of individual elements.

Borehole trajectory	Grid points# gas wells thru in lateral direction	Distance to panel 1 (m) [left]	Distance to the pillar centerline (m)	Distance to panel 2 (m) [right]
1	73	7.5	−17.5	–
2	81	–	2.5	22.5
3	83	–	7.5	17.5
4	85	–	12.5	12.5
5	87	–	17.5	7.5

Note: For distance to the pillar centerline, negative and positive values represent that the well is drilled to the left and right side of the pillar centerline, separately.

and the left panel (panel 1) was excavated first. These displacements and strains are then recorded before the right panel (panel 2) is subsequently excavated. Displacements are recorded throughout but are analyzed for potential well trajectories that pierce the remaining 50 m wide coal pillar. These are at nodes 73, 81, 83, 85 and 87 from the left to right in the lateral direction, respectively (Fig. 1). The five wells penetrate the pillars at distances from the flanked panels and the centerline of pillar as defined in Fig. 1 and Table 2.

3.3. Scenario design

We examine two scenarios using this geological model that incorporates topography, all for alternating beds of soft shale and stiff sandstone and with weak interfaces. These are for cases both (i) without and (ii) with topography. In each of the two scenarios there are three subscenarios representing panels at depths of 100, 200 and 300 m either below ground surface or the valley floor (Table 3). These results are discussed in the following.

4. Analysis and discussion of model results

Well failures due to shear, distortion, tension or compression are caused by strata movements after the twin panels are sequentially removed. Three zones usually develop over the gob after the extraction of the panels as long as the overburden is sufficiently thick. These are the caved zone, a fractured zone and zone of continuous deformation, respectively (Bai and Elsworth, 1990; Palchik, 1989; Peng, 1992). Overburden loading is transmitted through the remnant pillar and the side flanking coal and is sustained by underburden after mining. Even though the gas well is located within the pillar, which can provide certain protection for the well, various patterns of deformation, including shear, distortion, compression and tension, still occur within the surrounding rock of the well above the pillar.

To define the likely impact of longwall mining on the integrity of wells, the following first examines the magnitudes of shear offsets and bed separations experienced by wells in the overburden — by shear offset and delamination at the interfaces and, by inference, shearing and stretching of the casing. We then explore other modes of distress including vertical compaction where longitudinal shear strains along the well may be large. The wellbore trajectories are all vertical and extend from the surface to a depth of 300 m below the mined panel. We presume that these deformations are independent of the presence of any wellbores.

4.1. Magnitudes and distribution of shear offsets

We compare lateral shear offset (ΔU) (Fig. 2) at the interface between alternating monolithic shales and sandstones for both a horizontal surface and for incised topography. In each of these cases, mining is at the three depths of 100 m, 200 m and 300 m below the valley-base/ground-surface and involves the removal of the first one panel (left), followed by the other (right) and leaving a remnant intervening pillar. Profiles of shear offsets for the five well trajectories through this pillar in the two scenarios are shown in Figs. 4 and 5, with magnitudes of shear offsets for sub-scenarios listed in the summary table — Table 4.

4.1.1. Horizontal surface

As shown in Fig. 4 and Table 4, horizontal shear offsets increase as the seam deepens after either panel 1 or both panels are removed. After removing panel 1, most of the lateral offsets (for paths 2 to 5) are less than 100 mm. The largest offsets are for path 1 (closest to the rib of panel 1) and occur at the surface when mining is shallow (100 m), and migrate to the shallow roof (20–30 m above the seam) when mining is deeper (>100 m). As panel 2 is mined, ranges of shear offsets are −94–104 mm, −142–119 mm and −166–134 mm (Table 4) for seam depths of 100, 200 and 300 m, respectively. The sense of shear distortion in the beds reverses from counterclockwise to clockwise at some heights along these vertical wells, especially for paths 2 to 5 penetrating shallower seams, which are illustrated in Fig. 6. The positive offsets recover partially (Fig. 6(b)) but are replaced by even larger negative offsets when the second panel is removed (Fig. 6(c)). Shear offsets are largest for paths closest to the twin mined panels (paths 1 and 5) and reach a peak in the shallow roof (10–20 m above the seam). Path 2, which is closest to the center of the pillar, has the smallest resulting offsets after the twin panels are removed.

We note that the annular space between the production casing and the coal protection casing in the design used in practice allows for 150 mm, for the sake of safety, we limit the threshold of the annular space to 100 mm in the modeling design. This threshold, corresponding to the maximum allowable horizontal shear offset (both the positive and negative ones — ±100 mm), is indicated by the dashed lines in Figs. 4 and 5. The gas well is most likely to shear at heights where shear offsets exceed ±100 mm.

4.1.2. Incised valley topography

For wells penetrating overburden with incised valley topography the resulting wellbore deformation is similarly also represented as horizontal sliding and longitudinal distortion as wells move with the overburden. As the seam depth increases the ranges of lateral shear offsets for wells in the overburden below the valley are 39–188 mm, 31–206 mm and 19–215 mm for seam depths at 100, 200 and 300 m respectively after panel 1 is removed, and are reset to −161–134 mm, −180–145 mm and −203–154 mm after the removal of panel 2. The maximum offsets are larger than those for a horizontal surface — the

Table 3
Scenarios of numerical modeling for topographic influence on stability for gas wells.

Scenario		Topography (hill thickness/m)	Thickness of overburden (below the valley-base)/m	Ratio of hill thickness to that of overburden below the valley
i	1	–	100	–
	2	–	200	–
	3	–	300	–
ii	4	300	100	3.0
	5	300	200	1.5
	6	300	300	1.0

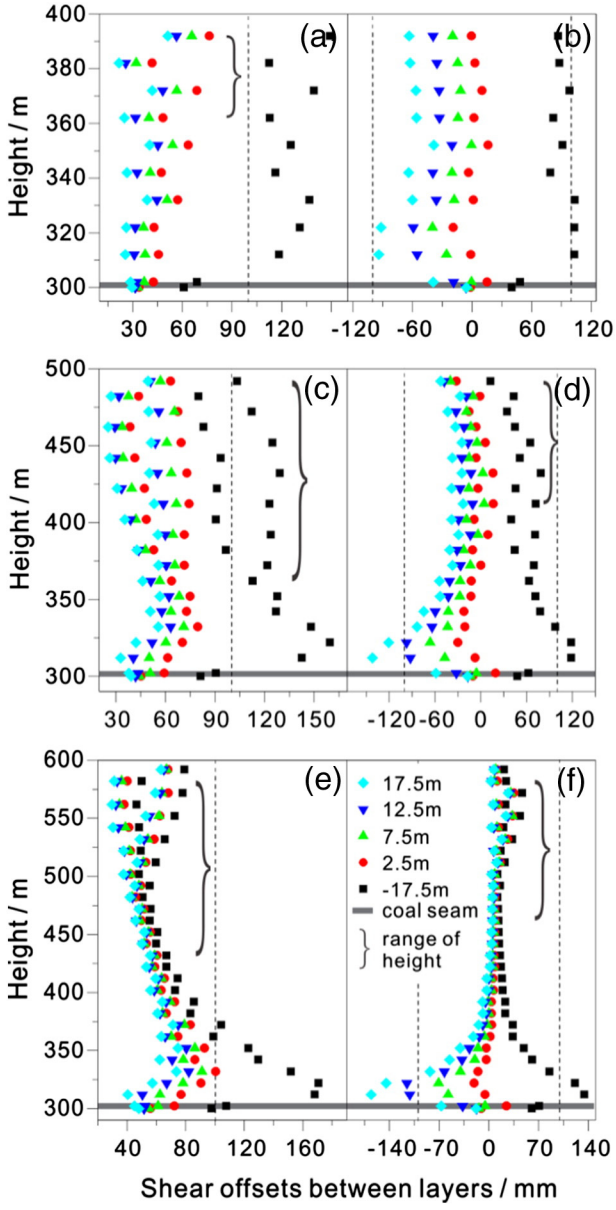

Fig. 4. Shear offsets (ΔU) at interfaces for the five candidate paths of wellbores in scenario (i) (seam at three depths of 100, 200 and 300 m below the horizontal ground surface), induced above a longwall pillar flanked by panels at depths of 100 m (a, b), 200 m (c, d) and 300 m (e, f) due to the mining of panel 1 to the left (a, c, e) and then panel 2 to the right (b, d, f). Seam is at the vertical ordinate of 300 m on plots (a)–(f). The range of height where delaminations occur is indicated by the right bracketed region ("}").

magnitudes are amplified by about 20–30% by the incised topography (Table 4). The larger the ratio of hill height to the thickness of overburden below the valley, the larger the shear offsets are amplified for wells below the valley. Also in this case, the larger shear offsets are induced near the crest of the hill. The enhanced shear effect on the wellbore induced by the addition of topography are mitigated as the seam deepens. However, magnitudes of shear offsets for wells within the hill are relatively smaller, especially for wells through deeper seams (100 m), of which the offsets are all less than ±100 mm (Table 4). When mining is shallow (100 m, with the max ratio = 3), as noted above, a few large offsets still arise near the hillcrest after coal mining (Fig. 5(a) and (b)). Shear offsets are largest in the shallow roof (10–30 m over the seam) and also above the pillar edges. Interior to this, shear offsets reduce sharply, most of which are less than ±100 mm.

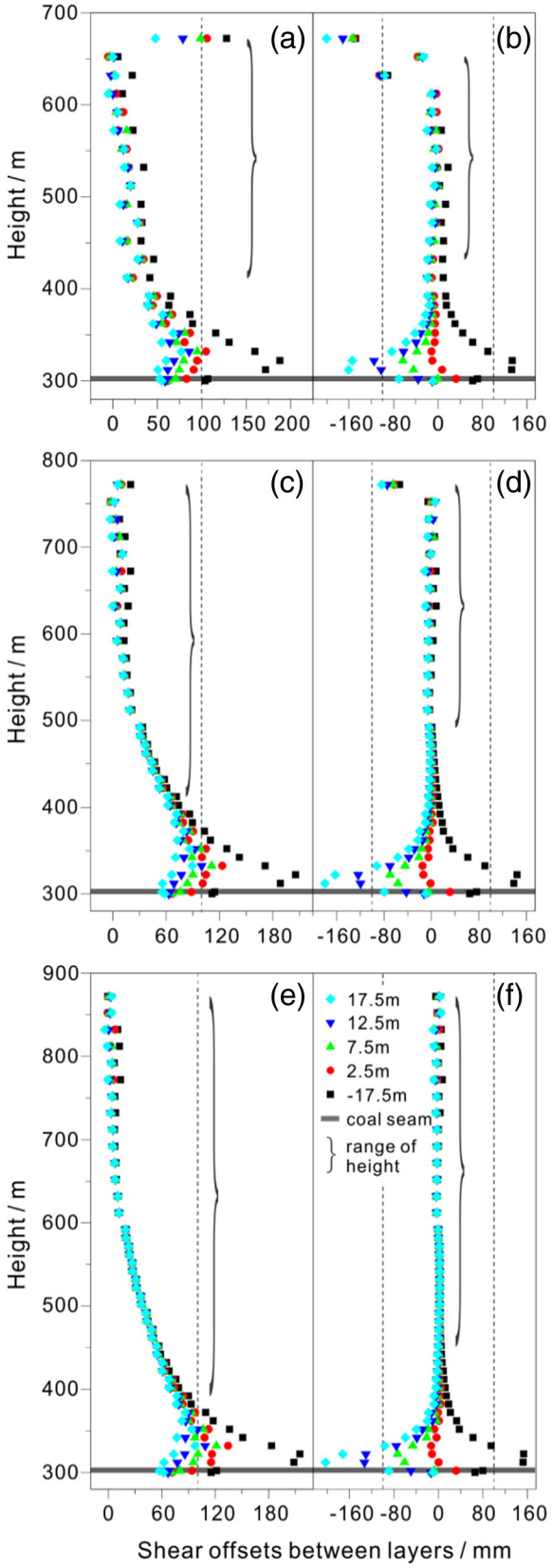

Fig. 5. Shear offsets (ΔU) at interfaces for the five candidate paths of wellbores to examine the effects of topography (scenario (i) — with incised valley topography and seam at three depths of 100, 200 and 300 m below the valley-base), induced above a longwall pillar flanked by panels at depths of 100 m (a, b), 200 m (c, d) and 300 m (e, f) due to the mining of panel 1 (a, c, e) and then panel 2 (b, d, f). Seam is at the vertical ordinate of 300 m on plots (a)–(f). The range of height where delaminations occur is indicated by the right bracketed region ("}").

Table 4
Statistical comparison of variation range of shear offsets in different scenarios after the removal of panel 1 and then panel 2.

Scenario		Thickness of overburden/m	Panel 1	Range of shear offsets/mm		
				Percentage change	Panels 1 and 2	Percentage change
i	1	100	22–149	–	−94–104	–
	2	200	25–160	–	−142–119	–
	3	300	30–171	–	−166–134	–
ii	4	300	−5–128	–	−200–19	–
		100	39–188	77%–26%	−161–134	71%–29%
	5	300	−3–22	–	−84–9	–
		200	31–206	24%–29%	−180–145	27%–22%
	6	300	−4–14	–	−9–7	–
		300	19–215	−37%–26%	−203–154	22%–15%

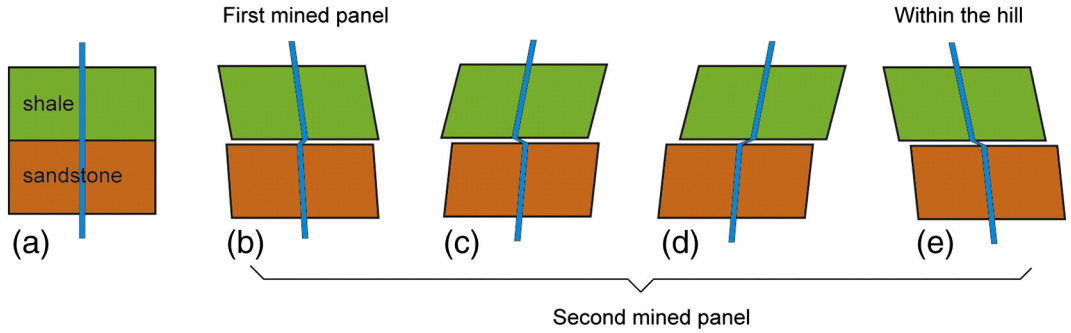

Fig. 6. Schematic diagrams of well (rock beds) deformations due to sequentially mining of panel 1 and panel 2 in various scenarios with slip interface between alternating layers both without and with topography, (a) a single well passing through layers before removing panels, (b) then deformed after the removal of panel 1, (b)–(e) then showing the recovered and then even the reversed well (rock beds) deformation in various degrees after the sequential removal of panel 2, and the deformation in (e) only occurs for wells penetrating layers within the hill.

4.1.3. Statistical analysis of large shear offsets

A well would likely not survive an offset greater than its diameter if applied over a short (i.e. less than one about diameter) vertical interval. In order to further analyze the topographic influence of shear-slippage caused by coal mining on well-survival, we aggregate separately the number of weak interfaces (N_{LSO}) at which larger shear offsets occur along the trajectory of a well in each sub-scenario. As noted above, the threshold, corresponding to the maximum allowable horizontal shear offset, is limited to 100 mm, here we define the threshold for the "largest shear offset" (LSO) with the same value. The aggregating rule is as follows: define the lateral displacement of node (i, j) as U_{ij}, and the lateral displacement for node $(i, j+1)$ as $U_{i(j+1)}$. Then, if $|\Delta U| = |U_{i(j+1)} - U_{ij}|$ 100 mm, then $N_{LSO} = N_{LSO} + 1$. After calculating this we obtain the results shown in Figs. 7 and 8, for scenarios 1 and 2, separately. In Figs. 7 and 8, the data linked by the solid line refer to N_{LSO} for wells after only panel 1 is removed and those linked by a dashed line are for wells after both panels are sequentially mined.

When the ground surface is flat (Fig. 7), well trajectory 1, which is closest to the left panel, has the largest number of hazardous interfaces at which the LSOs occur after panel 1 is extracted, while N_{LSO} reduces sharply as the well is located progressively further from the left panel. As panel 2 is excavated, both well trajectories 2 and 3, which are close to the center of the pillar, have the least number of ($N_{LSO} = 0$) high-risk interfaces. For incised topography, in the overburden below the valley (Fig. 8(a)), the distribution of N_{LSO} is similar to that for the horizontal case, but more high-risk interfaces arise for candidate paths 2–5. In addition, the magnitudes of shear offsets also enlarge (Table 4), indicating that the presence of topography significantly increases the risk of shear-instability for wells. For wells within the hill, the magnitudes of shear offsets decrease sharply as the seam deepens with only a few high-risk interfaces arising for wells piercing the shallowest seam (100 m, Fig. 5(a) and (b)). When mining is deeper (100 m), magnitude of offsets are much smaller compared with that occur in the overburden below the valley (Fig. 5(c)–(f)).

In general, it seems that there are more heights at which gas wells are prone to shear when penetrating shallower seams (Figs. 4, 5, 7 and 8), though these shear offsets are usually less than those for wells piercing deeper seams. This conforms to Karacan and Olea's result (Karacan and Olea, 2013), indicating that gob gas ventholes (GGVs) located at lower surface elevations might be more productive than those drilled through thicker overburden, because more fractures are formed and the permeability and transmissibility of these fractures are higher within a thinner overburden, which also indirectly reflects the extent of rock damage.

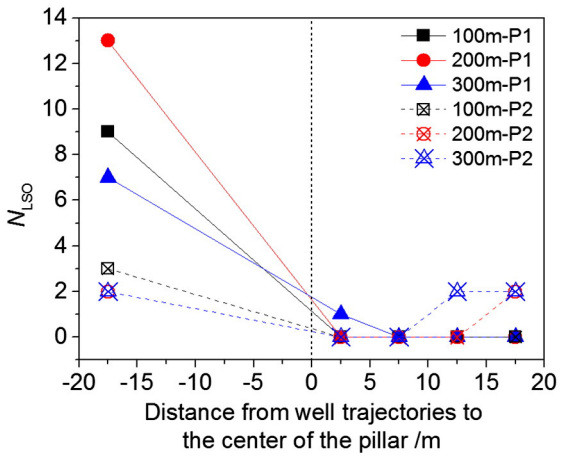

Fig. 7. Statistical results of the LSOs that occur at weak interfaces between alternating layers for a horizontal surface with no topography (scenario (i)) after the mining of the first panel (solid line) then both (dashed line) panels.

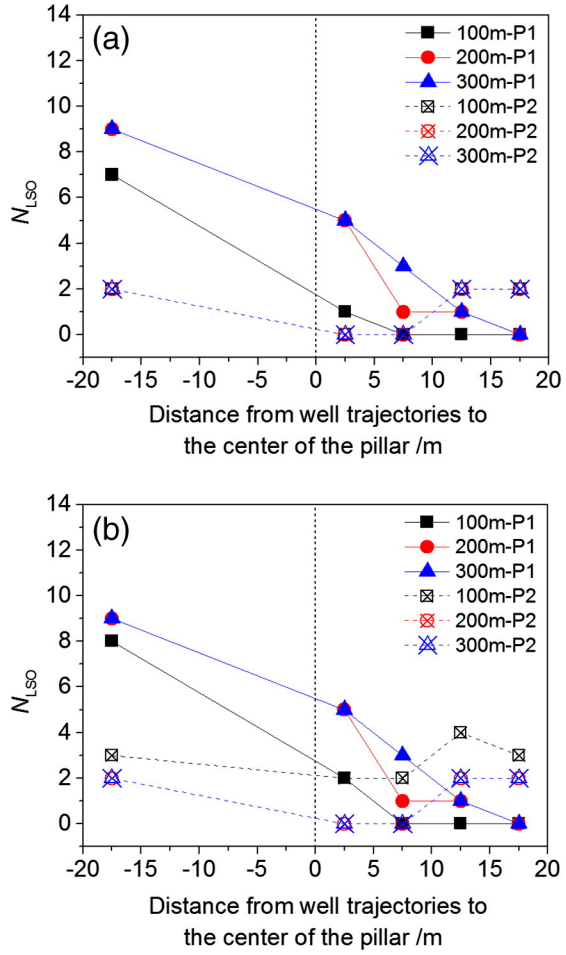

Fig. 8. Statistical results of LSO that occur at weak interfaces between alternating layers for mining with topography (scenario (ii)) after the mining of the first panel (solid line) then both (dashed line) panels.

4.2. Magnitudes and distribution of delaminations

Delaminations occur at weak planes between layered strong and weak strata due to their different physical characteristics and also influence the stability of gas wells (Palchik, 2005). We compare the delamination displacement (Δd) (Fig. 2) at the interface between alternating monolithic shales and sandstones for both a horizontal surface and for incised topography. Magnitudes and distribution of delamination for each scenario are tabulated in Table 5, and the range of height where bed separation occurs along the five well trajectories is also indicated by the right bracketed region ("}") in Figs. 4 and 5.

For wells penetrating overburden with a horizontal surface, the maximum delamination increases with seam depth and the depth occurrence also deepens with seam depth after either panel 1 or both panels are removed. All the maximum delaminations, for seams at various depths (100, 200 and 300 m), occur within a depth of 100 m below the surface. The greatest delamination is 12 mm and occurs at a height of 220 m above the seam for the deepest seam (300 m). While the lowest height where delamination forms goes up after the second panel is mined because partial horizontal fractures which are relatively close to the seam (at lower heights) are compacted due to the removal of the second panel. For cases with incised topography, the maximum delamination usually forms at a depth less than 200 m below the hill-crest after either panel 1 or both panels are removed, and the depth decreases as the seam deepens. However, the deeper the seam, the smaller the value of the maximum delamination, which is opposite to cases with a horizontal surface. After the second panel is removed, values of the maximum delamination increase but the range of height where delaminations occur is reduced. The greatest delamination is 42 mm after the twin panels are removed when mining at a shallow depth (100 m) under the hill.

Large delaminations induce tensile deformation in the borehole and casing, so that gas wells are likely to experience tensile failure within the shallow strata (less than 100 m deep) for cases with a horizontal surface. In contrast, tensile failure is more likely to occur for wells piercing the overburden with incised topography, and especially for cases with a higher ratio of hill height to the thickness of the overburden below the valley.

We also observe a connection between the ratio (H/m) of distance between the seam and the interface where the delamination forms (H) to the seam thickness (m) (Table 5). The height at which separate horizontal fractures occur is 30–140 and 45–140 times the seam thickness (60–280 m and 90–280 m above the seam) after the removal of the first one and then both panels when mining under a horizontal surface. And the height increases to 45–285 and 65–285 times (90–570 m and 130–570 m above the seam), respectively, the seam thickness after the sequential extraction of the twin panels when mining under incised topography. It is generally believed that the height of the fractured zone varies significantly amounting to 20–100 times the seam thickness after mining, and this fracture height depends on the characteristics of the overburden, bed thickness, uniaxial compressive strengths of overlying layers, location of layer interfaces and the coal seam thickness (Palchik, 2003, 2005; Peng, 1992; Turchaninov et al., 1977). In our study, the lower bound of the height where horizontal fractures form conforms to the previous conclusion, while the upper bound is exceeded for cases with a horizontal surface and is dramatically exceeded for cases with incised topography. We surmise that, on the one hand, there are no thicker and stronger layers which can restrain the upward development of the delamination in our model; on the other hand, the incised valley topography will also generate more horizontal fractures at higher elevations within the overburden.

4.3. Magnitudes of longitudinal well distortions, lateral and vertical strains

We analyze the comparative longitudinal well distortions (ε_{xy}) that develop for different scenarios. These distortions are equivalent to changes in lateral displacement with depth. We also analyze the lateral and vertical strains (ε_{xx} and ε_{yy}) around wells which could generate tensile and compressive failure in the casing. Since strains cannot be

Table 5
Statistical results of delamination and its distribution for different scenarios after the removal of panel 1 and panel 2.

Scenario	Seam depth (m)	Panel 1				Panels 1 and 2			
		Max (mm)	Height/depth (m)	Range of height/depth (m)	H/m	Max (mm)	Height/depth (m)	Range of height/depth (m)	H/m
1	100	2	60/−40	60–90/−40	30–45	1	90/−10	90/−10	45
2	200	11	140/−60	60–190/−140	30–95	6	140/−60	110–190/−90	55–95
3	300	12	220/−80	130–280/−170	65–140	12	220/−80	160–280/−140	80–140
4	300 + 100	35	210/−190	110–370/−290	55–185	42	250/−150	130–350/−270	65–175
5	300 + 200	29	350/−150	110–470/−390	55–235	33	390/−110	190–470/−310	95–235
6	300 + 300	17	490/−110	90–570/−510	45–285	21	490/−110	150–570/−450	75–285

directly calculated by FLAC, a FISH subroutine has been designed to get these data. Model results are shown in Figs. 9–14 and Tables 6–8.

4.3.1. Longitudinal well distortions—ε_{xy}

For the case with a horizontal surface (Fig. 9 and Table 6), longitudinal well distortions fluctuate along the path of a well as the properties of strata alternate. The differences in magnitude between these five paths narrow as mining deepens. For shallower seams (300 m), shear strains developed for wells following path 1 are much larger than those of paths 2–5. The peak shear strains usually occur at the surface and in the shallow roof of the seam. Traversing in the lateral direction, magnitudes of shear strains are largest above pillar edges, reaching a maximum of -22–23×10^{-4}, or equivalent to -22–23 mm horizontal displacement within one 10 m thick bed. Interior to the edge of the pillar, shear strains reduce noticeably, which are less than $\pm 5 \times 10^{-4}$ for most of the length of these wells. Where incised topography is considered (scenario (ii)) (Fig. 10 and Table 6), magnitudes of shear strains for wells within the overburden below the valley are slightly smaller than those absent topography (scenario (i)). As for wells within the hill, longitudinal distortions are largest for the shallowest seam, and reduce sharply as the

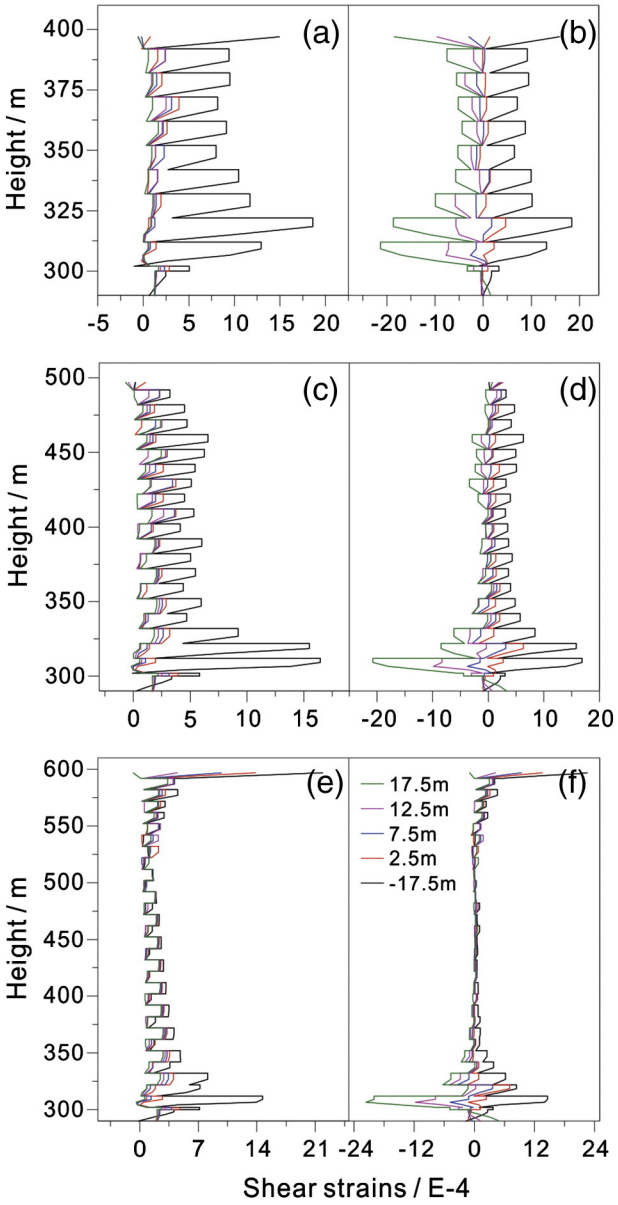

Fig. 9. Longitudinal well distortions (ε_{xy}) for scenario (i) (cases with a horizontal surface and the seam at three depths of 100, 200 and 300 m) due to the mining of the first panel to the left (a, c, e) followed by the second panel to the right (b, d, f).

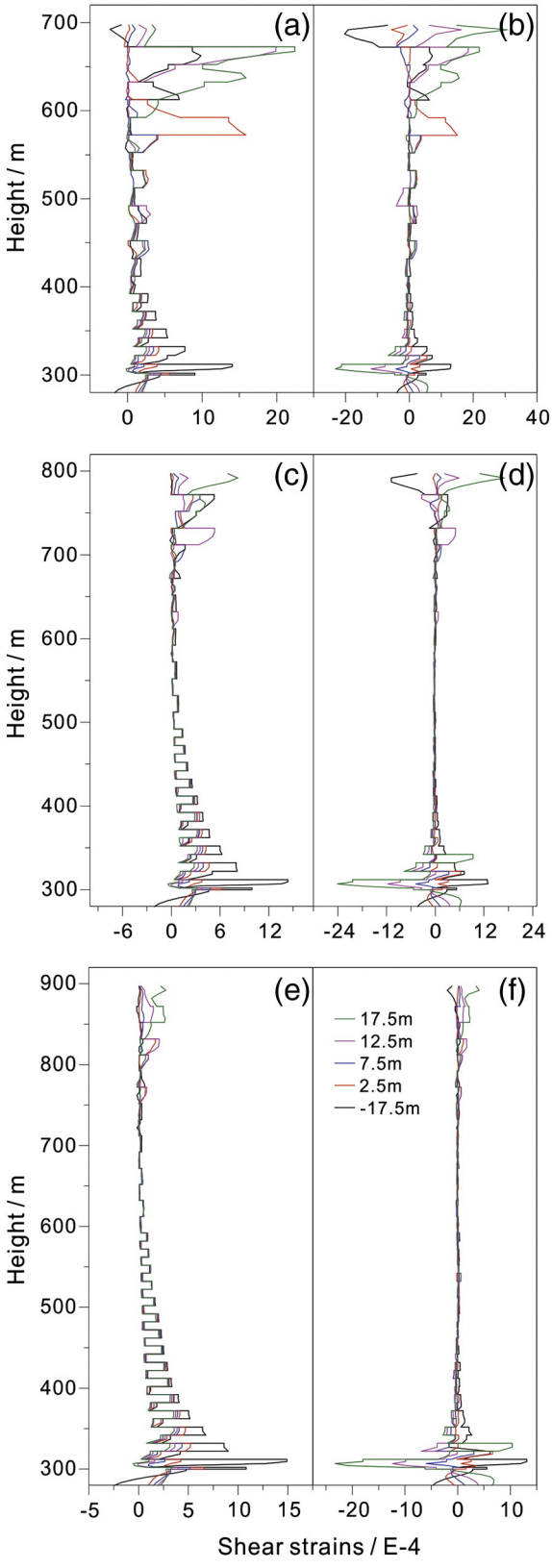

Fig. 10. Longitudinal well distortions (ε_{xy}) for scenario (ii) (cases with incised valley topography and the seam at three depths of 100, 200 and 300 m below the valley-base) due to the mining of the first panel to the left (a, c, e) followed by the second panel to the right (b, d, f).

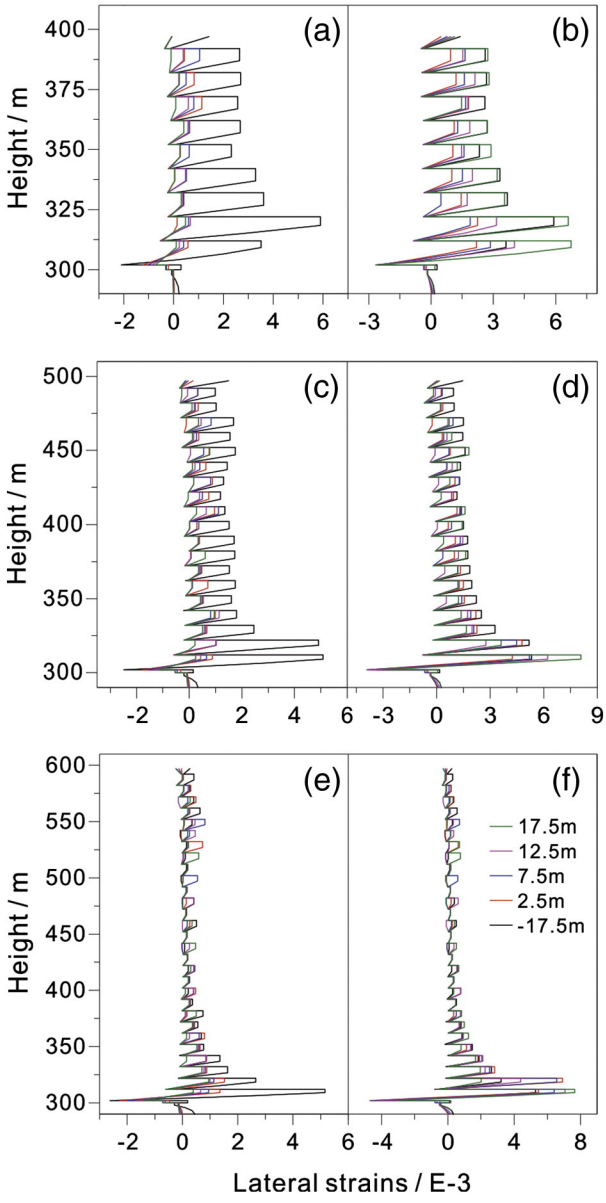

Fig. 11. Lateral strains (ε_{xx}) around wells for scenario (i) (cases with a horizontal surface and the seam at three depths of 100, 200 and 300 m) due to the mining of the first panel to the left (a, c, e) followed by the second panel to the right (b, d, f).

seam deepens. On the whole, the well distortions are largest near the hillcrest (for the shallower seam) and in the vicinity of the seam (for the deeper seam), which are all limited to ±3 millistrain. Incised valley topography does not result in a significant change in the magnitudes of longitudinal distortions along well trajectories over the case absent topography.

4.3.2. Lateral strains — ε_{xx}

The distribution and magnitudes of lateral strains in each sub-scenario are shown in Figs. 11, 12 and Table 7. For all cases, lateral strains are principally extensional along the vertical trajectory of the well after either one or both panels are removed. Lateral compressive strains only occur immediately above and below the pillar, and the differences in magnitude between these five paths also narrow as the seam deepens.

For cases with a horizontal surface, lateral strains are greatest around the seam, which are limited to ~6 millistrain in lateral extension and are less than ~3 millistrain in compression as panel 1 is removed.

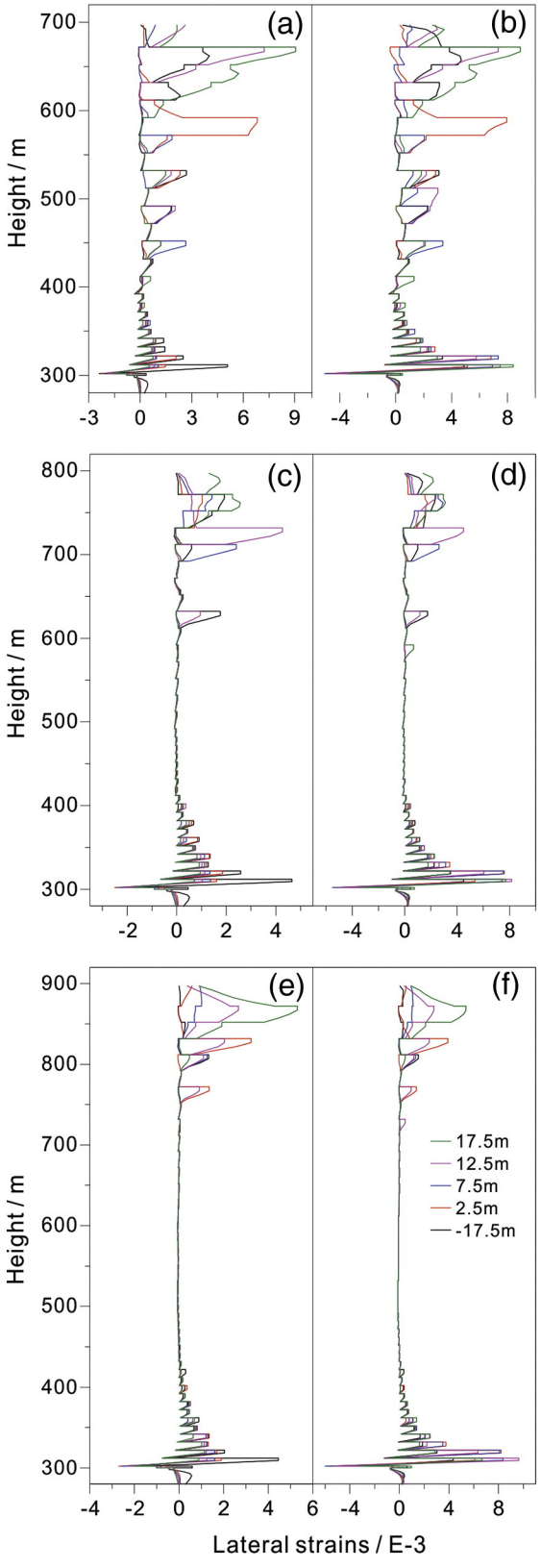

Fig. 12. Lateral strains (ε_{xx}) around wells for scenario (ii) (cases with incised valley topography and the seam at three depths of 100, 200 and 300 m below the valley-base) due to the mining of the first panel to the left (a, c, e) followed by the second panel to the right (b, d, f).

After the extraction of panel 2, lateral strains are amplified slightly with maximums of ~8 and ~5 millistrain in lateral extension and compression, respectively. For incised topography (scenario (ii)), the peak

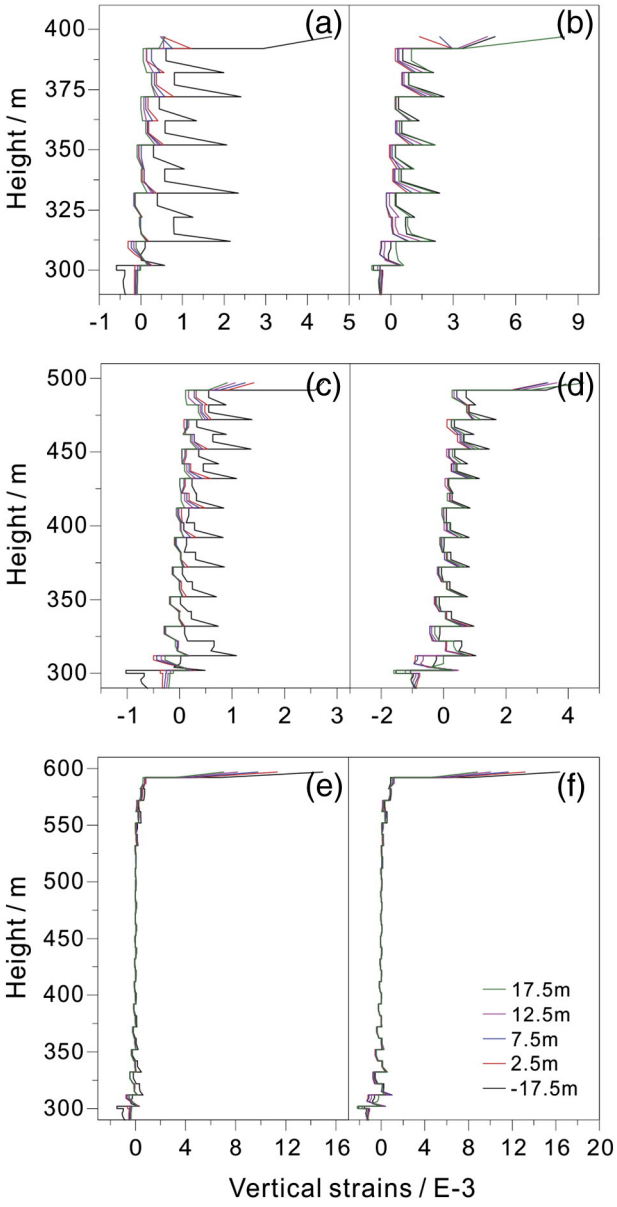

Fig. 13. Vertical strains (ε_{yy}) around wells for scenario (i) (cases with a horizontal surface and the seam at three depths of 100, 200 and 300 m) due to the mining of the first panel to the left (a, c, e) followed by the second panel to the right (b, d, f).

lateral strains occur around the seam and close to the hillcrest, which are separately limited to ~10 and ~6 millistrain in extension and compression for wells in the overburden below the valley, and are less than ~90 millistrain in extension within the hill. The incised topography results in only a small change in the magnitude of lateral strains (percentage changes are all less than ±15%) after panel 1 is removed, but results in a larger increase after the removal of panel 2. This is especially the case for lateral compression (increase 89% at most) and this effect is mitigated as the ratio of hill height to the thickness of the overburden below the valley is reduced.

4.3.3. Vertical strains — ε_{yy}

The distribution of vertical strains (Figs. 13, 14 and Table 8) is regular and similar between all the sub-scenarios. The overall trends are that vertical strains are largest both at the surface/hilltop where they are extensional and directly above and below the pillar where they are principally compressive, regardless of the topography. For cases with a horizontal surface, induced vertical strains are limited to ~3 millistrain

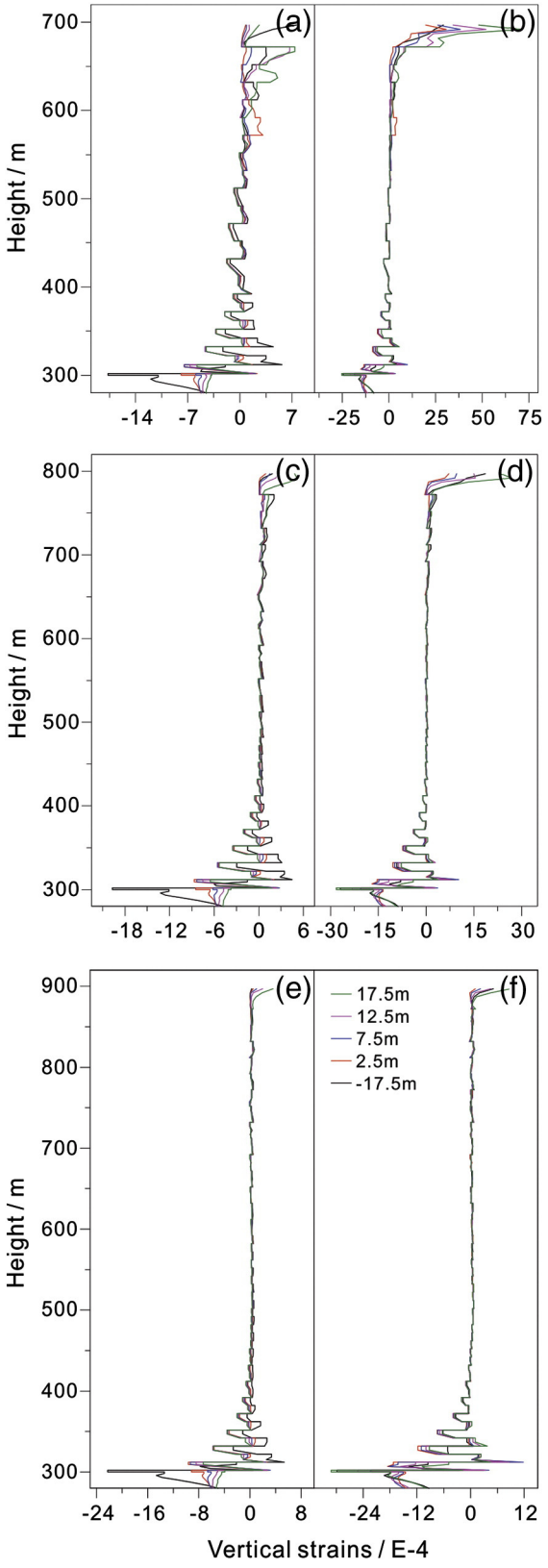

Fig. 14. Vertical strains (ε_{yy}) around wells for scenario (ii) (cases with incised valley topography and the seam at three depths of 100, 200 and 300 m below the valley-base) due to the mining of the first panel to the left (a, c, e) followed by the second panel to the right (b, d, f).

in compression and ~17 millistrain in extension after the extraction of both panels. Where topography is included (scenario (ii)), the greatest vertical tensile strains are ~7 millistrain within the hill and are

Table 6
Features of the distribution of longitudinal well distortions (ε_{xy}) above the coal seam after the removal of panel 1 and then panel 2 for different scenarios.

Scenario		Thickness of overburden/m	Range of ε_{xy}/E-4			
			Panel 1	Percentage change	Panels 1 and 2	Percentage change
i	1	100	−1–19	–	−21–18	–
	2	200	−1–16	–	−21–17	–
	3	300	−1–22	–	−22–23	–
ii	4	300	−2–22	–	−20–31	–
		100	−2–14	−26%	−23–13	−28%
	5	300	0–8	–	−11–17	–
		200	−3–14	−13%	−24–13	−24%
	6	300	0–3	–	−2–4	–
		300	−3–15	−32%	−23–13	−43%

Note: The percentage change in Table 6 is only for the positive shear strains, because the negative ones are relatively smaller as the first panel is removed, and there is almost no change in magnitude for the negative shear strains between cases with horizontal and incised topography after the second panel is removed.

Table 7
Features of the distribution of lateral strains (ε_{xx}) above coal seam after the removal of panel 1 and panel 2 for different scenarios.

Scenario		Thickness of overburden/m	Range of ε_{xx}/E-4			
			Panel 1	Percentage change	Panels 1 and 2	Percentage change
i	1	100	−21–59	–	−27–68	–
	2	200	−25–51	–	−39–81	–
	3	300	−26–52	–	−47–77	–
ii	4	300	−1–90	–	−4–89	–
		100	−24–51	14%–−14%	−51–84	89%–24%
	5	300	−1–43	–	−1–45	–
		200	−25–47	0–−8%	−55–82	41%–1%
	6	300	−1–53	–	−1–54	–
		300	−27–45	4%–−13%	−60–96	28%–25%

separately limited to ~3 and ~1 millistrain in vertical compression and extension for wells beneath the valley. Vertical compressive strains immediately above the seam are significantly elevated by the influence of the incised valley topography (increase 200% at most), while the tensile strains close to the hillcrest are much smaller compared with those near the surface when topography is absent (scenario (i); decrease 97% at most). Along almost the entire length of the well, except where it pierces layers near the surface or hillcrest and close to the seam, magnitudes of vertical strains for wells are principally of the order of 10^{-5}–10^{-4}.

5. Comparison with the previous studies

Few data are available to define the levels of distress experienced by wells undermined in the manner suggested here. In order to further evaluate the specific performance of wells and magnitudes of deformation under the impact of coal mining, especially for combining the influence of topography and weak interfaces, a comparison of this study is made against the results of the previous studies that address a subset of the issues examined here (topography, weak separations). These studies have evaluated axial strains along the well trajectories for longwall mining around a gas well at the Cumberland Mine in Pennsylvania (Luo et al., 1999; Vincent and Russell, 2013); deformations around a CNX well (Vincent and Russell, 2013); and evaluation of strains, displacements and distortions around a 2D longwall section with and without delamination and for a horizontal surface (Rostami et al., 2012). This latter study (Rostami et al., 2012) is augmented by this current study to examine the impacts of incised topography. The background for each study and the areas of overlap between them are tabulated in Table 9. We compare and contrast these studies in the following.

Seam depth, thickness and pillar widths are congruent in all the studies (Table 9) with impacts on the wells being the most severe in this most recent study that incorporates the most complex behavior. In prior work, vertical strains on the inner pipe of a well caused by shortening (Luo et al., 1999) are predicted to be 6×10^{-5} after the removal of the first panel and are magnified 10 times (6×10^{-4}) as the second panel is mined. However, these are significantly smaller than those caused by subsidence (Rostami et al., 2012) which are of the order of 10^{-4}–10^{-3}. Similarly, maximum shear offsets (Vincent and Russell, 2013) are of the order of 1.2–2.3 cm for various thicknesses of stiff beds (0.5–3 m), and are separately limited to ±10 cm and ±20 cm in prior (Rostami et al., 2012) and current studies, in which layers are all

Table 8
Features of the distribution of vertical strains (ε_{yy}) above coal seam after the removal of panel 1 and panel 2 for different scenarios.

Scenario	Thickness of overburden/m	Range of ε_{yy}/E-4			
		Panel 1	Percentage change	Panels 1 and 2	Percentage change
1	100	−6–46	–	−9–83	–
2	200	−10–27	–	−16–45	–
3	300	−15–149	–	−22–164	–
4	300	−2–8	–	−3–71	–
	100	−18–6	200%–−87%	−25–10	178%–−88%
5	300	0–5	–	0–27	–
	200	−20–4	100%–−85%	−28–10	75%–−78%
6	300	−1–4	–	0–9	–
	300	−22–5	47%–−97%	−31–12	41%–−93%

Table 9
Comparison of lateral shear offsets, shear, lateral and vertical strains with the previous studies.

Study conducted by		Burial depth/m	Seam thickness/m	Pillar width/m	First mined panel				Second mined panel			
					Shear offset ΔU/cm	Shear strain/ε_{xy}	Lateral strain/ε_{xx}	Vertical strain/ε_{yy}	Shear offset ΔU/cm	Shear strain/ε_{xy}	Lateral strain/ε_{xx}	Vertical strain/ε_{yy}
Luo et al. (1999)		307	1.9	56	–	–	–	−6E−5	–	–	–	−6E−4
Su, 2009 (Vincent and Russell, 2013)		315	1.7	65	–	–	–	–	1.2–2.3	–	–	–
Rostami et al. (2012)	*Homogeneous*	300	2.0	50	0–1.2	0–1 E-3	−1–4 E-4	−2–0 E-4	0–3	0–3 E-3	0–2 E-3	−2–0 E-3
	Layered	300	2.0	50	−2–7	−2–7 E-3	−1–8 E-3	−5–2 E-3	−8–6	−8–6 E-3	−1–8 E-3	−8–10 E-3
This study with *delamination*	*Horizontal*	300	2.0	50	3–17	−1–22 E-4	−26–52 E-4	−15–149 E-4	−17–13	−22–23 E-4	−47–77 E-4	−22–164 E-4
	Incised	300 + 300	2.0	50	2–22	−3–15 E-4	−3–5 E-3	−2–0 E-3	−20–15	−23–13 cE-4	−6–10 E-3	−3–1 E-3

Note: In Rostami et al. (2012), "*homogeneous*" refers to homogeneous strata without a deformability contrast between alternating layers and "*layered*" refers to the case of alternating 10 m thick monolithic beds of alternating high and low moduli but under conditions that neglect delamination or shear slip (bonded interface). In these two scenarios the shear offset (ΔU) is equal to the bed thickness multiplied by local distortion (shear strain). In this study with "*delamination*" we refer to the cases discussed here with bed-delamination and slip for geometries with a "*horizontal*" surface and those with "*incised*" topography.

10 m thick. Thus it may be surmised that shear offset is positively related with bed thickness. Compared to the case where delamination and slip on bed interfaces are not suppressed (this study), peak lateral shear offsets double under the effect of weak contacts (horizontal topography; Table 9), and further increase as influenced by incised topography (incised topography; Table 9). Shear strains in the strata (this study) are reduced over the layered case (Rostami et al., 2012), we surmise that bedding slip dissipates the magnitudes within the solid media. Strains in lateral extension and vertical compression decrease due to bedding slip and separation, respectively, while strains in lateral compression and vertical extension increase.

6. Conclusions

Gas wells that penetrate mineable coal seams may be subject to distress caused by ground movements due to longwall mining. Especially important are the lateral shear offsets and axial distortion, which are most damaging for wellbores. To replicate typical conditions in the Appalachian basin, a geological model that considers the combined effects of topography, weak interfaces between monolithic beds and various mining depths is presented in the foregoing. These conditions adequately represent the principal features of the anticipated response of gas wells that are near-undermined by longwall panels. We examine the magnitudes of longitudinal distortions, lateral shear offsets, delaminations, and vertical and lateral strains along vertical wells drilled to intersect the seam at various locations within the longwall pillar. We analyze the distribution of these deformations and predict areas where the most severe deformation would occur. Based on this work, the influence of topography and the presence of monolithic beds with weak interfaces are examined with respect to their influence on the resulting deformation field and the likelihood for the survival of gas wells, so affected. Through this study, the following conclusions are drawn:

(1) The principal mechanisms of wellbore distress for gas wells penetrating the longwall pillar is mainly in response to horizontal sliding between layers and axial distortion as wells move with overburden. These are the two principal deformation patterns which promulgate large strains that may be sufficient to induce failure of wellbores and contained well casings. In contrast, much smaller axial distortion of wells results from distortion in the beds and more gradual changes in lateral displacements.

(2) Incised topography generates significant impacts on well deformations over the case of an assumed horizontal ground surface. Compared with wells drilled vertically through strata with horizontal surface, the magnitudes of shear offsets for wells in the overburden but below the valley are amplified about 20–30%. The larger the ratio of hill height to the thickness of overburden below the valley, the larger the amplification of the shear offsets. The largest shear offsets for a horizontal surface do not exceed 170 mm and are limited to 220 mm for cases with incised topography.

Well distortions are largest close to the surface/hilltop for mining at shallow depths (~100 m) and migrate downwards with an increase in panel depths (>100 m). These reach a maximum in the vicinity of the seam but also reduce in magnitude with an increase in seam depth. Incised topography does not cause a significant change in magnitude for longitudinal distortions along well trajectories, which are all limited to $\pm 3 \times 10^{-3}$. Lateral strains are greatest in the vicinity of the seam for cases with a horizontal surface (-5–8×10^{-3}) and are largest around the seam and close to the hilltop for incised topography (-6–10×10^{-3}). Incised topography causes only a mild change in lateral strains following the removal of panel 1 (percentage changes are all less than $\pm 15\%$), but an apparent increase after the removal of the second panel (percentage changes are around 30%). For incised topography, vertical compressive strains immediately above

the seam are much larger than for the horizontal surface reaching a peak magnitude of -3×10^{-3}, while the peak vertical tensile strains close to the hillcrest are much smaller compared with those near the horizontal surface ($\sim1.6\times10^{-2}$).

(3) Irrespective of whether the topography is incised or horizontal, well deformations (lateral shear offsets and various strains) are largest in the lateral direction for boreholes that cross the pillar closest to the panel rib. These ensemble deformations reduce monotonically towards the gateroad, where both the shear offsets and axial distortions reduce to about one-fifth (horizontal) and one-tenth (incised) of the maximum at 7.5 m inboard of the gateroad. In the vertical direction, wells are prone to failure in layers around the seam and close to the ground or hillcrest surface. Well deformations are most severe when mining is shallow (<100 m), then moderate when mining at an intermediate depth (~200 m), and then become large again as the seam deepens (>300 m). The spread in the distribution of strain magnitudes between the five horizontal trajectories through the pillar all narrow when mining is deeper.

(4) Tensile failure is another pattern of wellbore instability which may occur between delaminating layered strong and weak strata, due to the presence of large delamination deformations along these weak interfaces after the sequential excavation of panels. The largest delamination deformations are 12 and 42 mm after the twin panels are removed when mining under a horizontal surface and an incised valley topography, respectively. Gas wells penetrating overburden with incised topography are relatively more likely to fail in tension, especially for the case with a higher ratio of hill thickness to that of overburden below the valley. The peak delamination deformations decrease for cases with a horizontal surface but increase for cases with incised topography due to the removal of the second panel.

(5) Sequential extraction of the twin panels flanking the coal pillar also engenders different impacts on well stability. That is, after the removal of the second panel, the initial positive shear offsets resulting from the removal of the first panel are reset and even overridden by larger negative offsets — resulting in a net distortion of negative sense. Both the extensional and compressive lateral and vertical strains increase after the extraction of the second panel.

(6) Through comparison with other studies, we find that shear offset is positively correlated with the thickness of the monolithic beds comprising the overburden. Incorporating inter-layer slip between beds is important as otherwise predicted shear offsets may be only half of the correctly predicted offsets with slip.

(7) These analyses inform methods of mitigating casing distress and elevating survivability of wells — these include strengthening the strata in shallow regions, potentially by grouting, destressing these areas, or over-reaming wellbore diameters and soft-grouting in casing with a soft sacrificial annulus to allow the accommodation of shear offset while still retaining an open hole section that can accommodate the central casing stem.

Acknowledgments

Financial support for this work is provided by the State Key Laboratory of Coal Resources and Mine Safety, China University of Mining and Technology (No. SKLCRSM12X01), the Program for Postgraduate Research Innovation in Universities of Jiangsu Province (No. CXZZ12_0951), and the China Scholarship Council (201206420029). This support is gratefully acknowledged. We are also grateful to editor C. Özgen Karacan and the two anonymous reviewer for their valuable comments which helped to improve the paper.

References

Aadnoy, B.S., 1988. Modeling of the stability of highly inclined boreholes in anisotropic rock formations. SPE Drill. Eng. 259–268.
Aadnoy, B.S., Chenevert, M.E., 1987. Stability of highly inclined boreholes (includes associated papers 18596 and 18736). SPE Drill. Eng. 2, 364–374.
Ajalloeian, R., Lashkaripour, G.R., 2000. Strength anisotropies in mudrocks. Bull. Eng. Geol. Env. 59, 195–199.
Aoki, T., Tan, C.P., Bamford, W.E., 1993. Effects of deformation and strength anisotropy on borehole failure in saturated shales. Int. J. Rock Mech. Min. Sci. Geomech. 30, 1035–1038.
Ardeshiri, S., Yazdani, M., 2008. Numerical study of fault geometrical effects on seismic stability of large underground caverns. The 42nd US Rock Mechanics Symposium and 2nd U.S.-Canada Rock Mechanics SymposiumARMA, American Rock Mechanics Association, San Francisco.
Bai, M., Elsworth, D., 1990. Some aspects of mining under aquifers in China. Min. Sci. Technol. 10 (1), 81–91.
Bennion, D.B., Thomas, F.B., Bietz, R.F., 1996. Low permeability gas reservoirs: problems, opportunities and solutions for drilling, completion, stimulation and production. SPE Gas Technology SymposiumSociety of Petroleum Engineers, Inc., Calgary, Alberta, Canada, pp. 117–131.
Bjornsson, E., Hucik, B., Szutiak, G., Brown, L.A., Evans, H., Curry, D., Perry, P., 2004. Drilling optimization using bit selection expert system and ROP prediction algorithm improves drilling performance and enhances operational decision making by reducing performance uncertainties. SPE Annual Technical Conference and Exhibition. Society of Petroleum Engineers, Houston, Texas, pp. 1–6.
Bradley, W.B., 1979. Failure of inclined boreholes. J. Energy Resour. Technol. 101, 232–239.
Burrel, R., Friel, S., 1996. The effect of mine closure on surface emission. Proc Conf Environmental Management of Mine Operations. IBS, London.
Chen, J., Wang, T., Zhou, Y., Zhu, Y., Wang, X., 2012. Failure modes of the surface venthole casing during longwall coal extraction: a case study. Int. J. Coal Geol. 90–91, 135–148.
Chenevert, M.E., Gatlin, C., 1965. Mechanical anisotropies of laminated sedimentary rocks., pp. 67–77.
Clancey, B., Khemakhem, A.S., Bene, T., Schmidt, M., 2007. Design, construction and optimization of big-bore gas wells in a giant offshore field. SPE/IADC Drilling Conference, Amsterdam, The Netherlands, pp. 1–9.
Donath, F.A., 1964. Strength variation and deformational behavior in anisotropic rock. State of Stress in the Earth's Crust, pp. 281–298.
Elsworth, D., Liu, J., 1995. Topographic influence of longwall mining on ground-water supplies. Ground Water 33, 786–793.
Gebauer, A., Kroner, C., Jahr, T., 2009. The influence of topographic and lithologic features on horizontal deformations. Geophys. J. Int. 177, 586–602.
Gough, D.I., Bell, J.S., 1981. Stress orientations from oil-well fractures in Alberta and Texas. Can. J. Earth Sci. 18, 638–645.
Gutierrez, J.J., Vallejo, L.E., Lin, J.S., 2010. A study of highway subsidence due to longwall mining using data collected from I-79. Pennsylvania Department of Transportation (Contract #510601).
Haimson, B.C., Song, I., 1993. Laboratory study of borehole breakouts in Cordova Cream: a case of shear failure mechanism. Int. J. Rock Mech. Min. 30, 1047–1056.
Hale, A.H., Mody, F.K., Salisbury, D.P., 1993. The influence of chemical potential on wellbore stability. SPE Drill. Complet. 8 (3), 207–216.
Itasca Ltd., 2002. FLAC2D, User's Manual. Itasca Consulting Group, Inc.
Karacan, C.Ö., 2009a. Forecasting gob gas venthole production performances using intelligent computing methods for optimum methane control in longwall coal mines. Int. J. Coal Geol. 79, 131–144.
Karacan, C.Ö., 2009b. Reconciling longwall gob gas reservoirs and venthole production performances using multiple rate drawdown well test analysis. Int. J. Coal Geol. 80, 181–195.
Karacan, C.Ö., 2013. Integration of vertical and in-seam horizontal well production analyses with stochastic geostatistical algorithms to estimate pre-mining methane drainage efficiency from coal seams: Blue Creek seam, Alabama. Int. J. Coal Geol. 114, 96–113.
Karacan, C.Ö., Goodman, G., 2009. Hydraulic conductivity changes and influencing factors in longwall overburden determined by slug tests in gob gas ventholes. Int. J. Rock Mech. Min. Sci. 46, 1162–1174.
Karacan, C.Ö., Olea, R.A., 2013. Sequential Gaussian co-simulation of rate decline parameters of longwall gob gas ventholes. Int. J. of Rock Mech. Min. Sci. 59, 1–14.
Karacan, C.Ö., Ruiz, F.A., Cotè, M., Phipps, S., 2011. Coal mine methane: a review of capture and utilization practices with benefits to mining safety and to greenhouse gas reduction. Int. J. Coal Geol. 86, 121–156.
Kral, V., Paletnik, M., Novotny, R., 1998. Methane from closed-down mines in the soil. Proc Int Conf Coal-Bed Methane Technologies of Recovery and UtilizationGIG, Katowice, Poland.
Lee, H., Ong, S.H., Azeemuddin, M., Goodman, H., 2012. A wellbore stability model for formations with anisotropic rock strengths. J. Pet. Sci. Eng. 96–97, 109–119.
Liu, J., Elsworth, D., 1997. Three-dimensional effects of hydraulic conductivity enhancement and desaturation around mined panels. Int. J. Rock Mech. Min. Sci. 34, 1139–1152.
Liu, J., Elsworth, D., 1999. Evaluation of pore water pressure fluctuation around an advancing longwall face. Adv. Water Resour. 22, 633–644.
Luo, Y., Peng, S.S., Zhang, Y.Q., 1999. Analysis of the observed failure on the inner tubing of gas well W-510 below the coal seam. College of Engineering and Mineral Resources, West Virginia University (May 24).
McLamore, R., Gray, k.E., 1967. The mechanical behavior of anisotropic sedimentary rocks. J. Eng. Ind. 62–73.

Niandou, H., Shao, J.F., Henry, J.P., Fourmaintraux, D., 1997. Laboratory investigation of the mechanical behaviour of tournemire shale (vol 34, pg 3, 1997). Int. J. Rock Mech. Min. Sci. 34, 3–16.
Ong, S.H., Roegiers, J.C., 1993. Influence of anisotropies in borehole stability. Int. J. Rock Mech. Min. 30, 1069–1075.
Palchik, V., 1989. Analytical and empirical prognosis of rock foliation in rock masses. J. Coal Ukraine 7, 45–46.
Palchik, V., 2003. Formation of fractured zones in overburden due to longwall mining. Environ. Geol. 44, 28–38.
Palchik, V., 2005. Localization of mining-induced horizontal fractures along rock layer interfaces in overburden: field measurements and prediction. Environ. Geol. 48, 68–80.
Peng, S.S., 1992. Surface subsidence engineering. Society for Mining, Metallurgy and Exploration Inc., Lilleton.
Ramamurthy, T., Rao, G.V., Singh, J., 1993. Engineering behavior of phyllites. Eng. Geol. 33, 209–225.
Rostami, J., Elsworth, D., Watson, R., 2012. Study of borehole stability for gas wells in longwall mining areas. Report Submitted to Range Resources.
Santarelli, F.J., Brown, E.T., Maury, V., 1986. Analysis of borehole stresses using pressure-dependent, linear elasticity. Int. J. Rock Mech. Min. 23, 445–449.
Supon, S.B., Adewumi, M.A., 1991. Experimental study of the annulus pressure drop in a simulated air-drilling operation: SPE Drilling Engng V6, N1, March 1991, P 74–80. Int. J. Rock Mech. Min. 28, A370.
Tan, C.P., Willoughby, D.R., 1993. Critical mud weight and risk contour plots for designing inclined wells. The 68th Annual Technical Conference and Exhibition of the Society of Petroleum Engineers, Houston, Texas, pp. 101–115.
Tan, C., Richards, B., Rahman, S.S., 1996. Managing physico-chemical wellbore instability in shales with the chemical potential mechanism. Asia Pacific Oil and Gas Conference, Adelaide, pp. 107–116.
Tan, C.P., Rahman, S.S., Richards, B.G., Mody, F.K., 1998. Integrated rock mechanics and drilling fluid design approach to manage shale instability. SPE/ISRM Rock Mechanics in Petroleum Engineering.
Tien, Y.M., Kuo, M.C., Juang, C.H., 2006. An experimental investigation of the failure mechanism of simulated transversely isotropic rocks. Int.J. Rock Mech. Min. Sci. 43, 1163–1181.
Turchaninov, I.A., Iofis, M.A., Kasparian, E.V., 1977. Principles of Rock Mechanics. Nedra, Leningrad.
Van Oort, E., Hale, A.H., Mody, F.K., Roy, S., 1994. Critical parameters in modeling the chemical aspects of borehole stability in shales and in designing improved water-based shale drilling fluids. Paper SPE, 28309, pp. 171–186.
Vincent, A.S., Russell, P.M., 2013. Industry research into gas and oil well protective coal pillar design. In 32nd International Conference on Ground Control in Mining, Morgantown, WV, pp. 45–52.
Wang, Y., Watson, R., Rostami, J., Wang, J., Limbruner, M., He, Z., 2013. Study of borehole stability of Marcellus shale wells in longwall mining areas. J. Petrol. Explor. Prod. Technol. 1–13.
Whittles, D.N., Lowndes, I.S., Kingman, S.W., Yates, C., Jobling, S., 2007. The stability of methane capture boreholes around a long wall coal panel. Int. J. Coal Geol. 71, 313–328.
Zeynali, M.E., 2012. Mechanical and physico-chemical aspects of wellbore stability during drilling operations. J. Pet. Sci. Eng. 82–83, 120–124.
Zheng, Z., Kemeny, J., Cook, N.G.W., 1989. Analysis of borehole breakouts. J. Geophys. Res. 94, 7171.
Zoback, M.D., Moos, D., Mastin, L., Anderson, R.N., 1985. Well bore breakouts and in situ stress. J. Geophys. Res. Solid Earth (1978–2012) 90, 5523–5530.